THE JOURNAL OF PHYSICAL CHEMISTRY Letters

pubs.acs.org/JPCL Letter

Resolving Enhanced Mn^{2+} Luminescence near the Surface of $CsPbCl_3$ with Time-Resolved Cathodoluminescence Imaging

Rebecca B. Wai, Namrata Ramesh, Clarice D. Aiello, Jonathan G. Raybin, Steven E. Zeltmann, Connor G. Bischak, Edward Barnard, Shaul Aloni, D. Frank Ogletree, Andrew M. Minor, and Naomi S. Ginsberg*

Cite This: J. Phys. Chem. Lett. 2020, 11, 2624−2629 Read Online

ACCESS | Metrics & More | Article Recommendations | Supporting Information

ABSTRACT: Mn^{2+} doping of lead halide perovskites has garnered recent interest because it produces stable orange luminescence in tandem with perovskite emission. Here, we observe enhanced Mn^{2+} luminescence at the edges of Mn^{2+}-doped $CsPbCl_3$ perovskite microplates and suggest an explanation for its origin using the high spatiotemporal resolution of time-resolved cathodoluminescence (TRCL) imaging. We reveal two luminescent decay components that we attribute to two different Mn^{2+} populations. While each component appears to be present both near the surface and in the bulk, the origin of the intensity variation stems from a higher proportion of the longer lifetime component near the perovskite surface. We suggest that this higher emission is caused by an increased probability of electron−hole recombination on Mn^{2+} near the perovskite surface due to an increased trap concentration there. This observation suggests that such surface features have yet untapped potential to enhance emissive properties via control of surface-to-volume ratio.

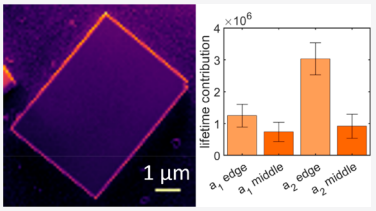

Mn^{2+} is a common, highly emissive semiconductor dopant that has been extensively studied, especially recently in metal halide perovskites.[1,2] Introducing Mn^{2+} dopants is a method for obtaining orange emission and enables simultaneous two color emission from the perovskite host matrix and the Mn^{2+} dopant (Figure 1a).[3−7] In this system, Mn^{2+} substitutes for Pb^{2+} in the perovskite crystal lattice (Figure 1b).[4,5,8] The Mn^{2+} ion provides a $^4T_1$ to $^6A_1$ transition, though its coordination and environment can alter the emissive properties. For example, Mn−Mn coupled pairs, formed at higher Mn^{2+} concentrations, alter the coordination environment and have been cited as a source for biexponential photoluminescence (PL) decay behavior in these materials.[9,10] Intriguingly, doping has previously been used to achieve desirable perovskite properties, such as stability of the preferred crystal structure.[11,12] While certain qualitative trends can be surmised from the literature, e.g., a red shift in the wavelength of the Mn^{2+} emission wavelength as a function of increasing Mn^{2+} concentration, quantitative inconsistencies remain.[4,7,9,10,13−16]

Many studies have previously focused on the luminescence properties of ensembles of Mn^{2+} doped $CsPbCl_3$ nanocrystals synthesized using various methods.[3−11,13,15−29] Yet ensembles of particles often have some distribution of properties, and ensemble average measurements can obscure information about variations within the sample. For example, nonuniformity in Mn^{2+} dopant concentration or dispersity in particle size or shape within or across different ensembles is a possible source of variation in photophysical properties. Energy dispersive X-ray spectroscopy (EDS) can be used to spatially characterize elemental composition and has previously been used to map Mn^{2+} distributions within perovskite materials.[7,8] The presence of Mn^{2+} alone, however, does not report on spatial variations in Mn^{2+} decay dynamics nor does the local concentration of Mn^{2+} obtained by EDS provide the concomitant spatial variation of Mn^{2+} luminescence properties. Ideally, to identify concentration, environment, and luminescence variations in Mn^{2+} doped perovskites, a combination of EDS and spatially resolved luminescence would be required.

Here, we use the capabilities of time-resolved cathodoluminescence (TRCL) imaging in combination with EDS to achieve a more detailed and spatially resolved understanding of the photophysical behavior of the Mn^{2+} dopant. Photoluminescence (PL) lifetimes are commonly used to detect small changes in the local environment of a luminescent species.[30] Fluorescence lifetime imaging (FLIM) combines the lifetime information with spatial resolution.[31,32] While valuable, optical diffraction-limited measurements make comparing surface and bulk properties a challenge. In cathodoluminescence (CL), a focused electron beam in a scanning electron microscope (SEM) generates electron and hole pairs that can radiatively recombine to produce luminescence (Figure 1c). To create an image, the electron beam (e-beam) is rastered

Received: February 20, 2020
Accepted: March 16, 2020
Published: March 19, 2020

https://dx.doi.org/10.1021/acs.jpclett.0c00574
J. Phys. Chem. Lett. 2020, 11, 2624−2629

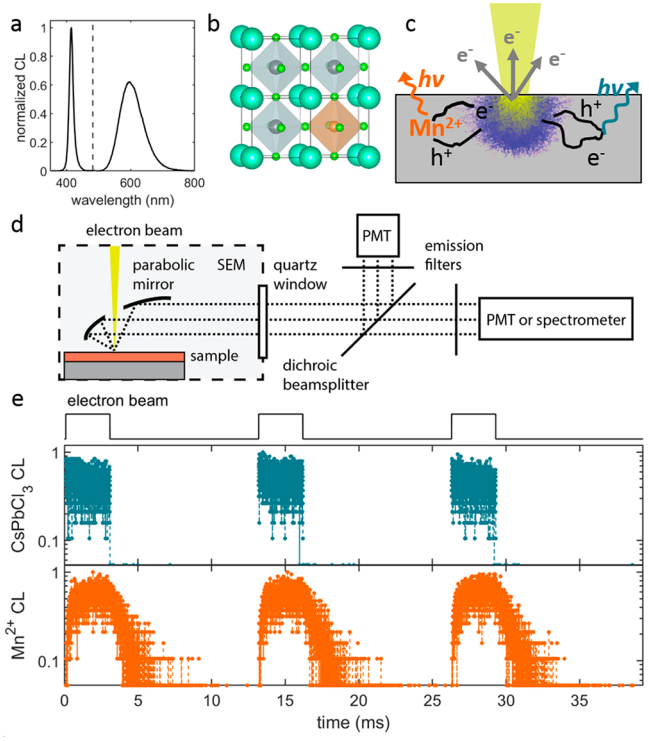

Figure 1. (a) Bulk CL spectrum of Mn^{2+} doped perovskite plates with the perovskite band edge emission at 415 nm and the broader Mn^{2+} emission at 595 nm. A filter at 482 nm was used to separate the two signals (dotted line). (b) Schematic showing the substitution of Mn^{2+} (orange) for Pb^{2+} (gray) in the perovskite lattice. (c) CL emission arising from the recombination of electrons and holes generated when electrons from a focused electron beam scatter within the sample. CL photons and secondary electrons are collected simultaneously. (d) CL detection apparatus, adapted from ref 33 with permission. (e) Electron beam duty cycle (top) with corresponding raw CL emission from the perovskite and the Mn^{2+} dopant.

across the sample, and the emitted light is collected in the far-field (Figure 1d), building up a spatial map in which each pixel value represents the luminescence due to the e-beam excitation of the sample. CL imaging has previously been used to measure spatially varying chemical composition of perovskite materials, including in halide demixing, dopant incorporation, and enhanced edge emission.[33−36] In other materials, CL has been used to identify regions of enhanced emission efficiency.[37] CL imaging provides superior, typically nanoscale, spatial resolution (a convolution of e-beam generation volume and sample-specific carrier diffusion length) and correlated secondary electron (SE) and CL images. These aspects of CL imaging are highly advantageous, yet CL images alone do not contain luminescence lifetime information.

Fortunately, time-resolved CL acquisition is also possible for photophysical characterization of luminescent samples and has previously been performed in perovskites.[38−40] We therefore use TRCL imaging to spatially characterize the Mn^{2+} dopant's emission at high spatial resolution. Unlike CL intensity imaging alone, TRCL imaging should be able to resolve variations in luminescence lifetime to report on variations in electronic structure or environment more sensitively than the spectral shift of the characteristically broad Mn^{2+} emission peak. Like FLIM, TRCL imaging should also be robust to many intensity-based imaging artifacts, potentially including geometry-associated changes in excitation density, photon escape probability, or acquisition geometry, which could affect the total intensity but not the relative contribution to the overall lifetime.

We measured TRCL on individual microplates of Mn:$CsPbCl_3$ (synthesis information in Supporting Information). The persistent rectangular shapes of the microplates are consistent with the possible orthorhombic, tetragonal, or cubic structure of the $CsPbCl_3$ perovskite (Figure 1b).[1] Although we did not explicitly measure the structure, the rectangular prism structure of the microplates could arise due to crystal

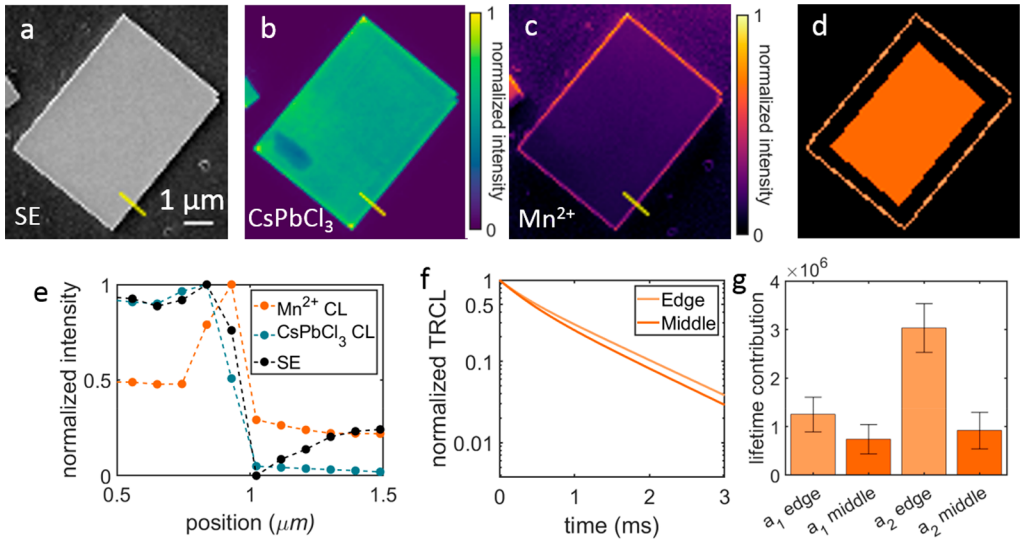

Figure 2. (a) Secondary electron (SE) and (b, c) cathodoluminescence (CL) images are given for a characteristic perovskite plate. (d) Images are segmented into edge (pale orange) and middle regions (orange) before the TRCL decays are fitted and deconvolved. (e) Linecuts across the yellow line on the images show that the change in Mn^{2+} CL intensity at the edge is more pronounced than changes in either the $CsPbCl_3$ CL intensity or the SE signal. (f) The deconvolved TRCL decay shows different decay behavior between edge and middle. (g) A bar plot of the fitted amplitudes for each lifetime is shown. The contribution of the longer lifetime a_2 changes between the edge and middle, while the contribution of the shorter lifetime, a_1, changes less.

https://dx.doi.org/10.1021/acs.jpclett.0c00574
J. Phys. Chem. Lett. 2020, 11, 2624−2629

formation on the substrate proceeding in both in-plane directions while only occurring in a single out-of-plane direction. Scanning transmission electron microscope (STEM) EDS characterization shows 1 atom % Mn^{2+} doping. The bulk CL emission spectrum of the microplates shows emission from $CsPbCl_3$ at 415 nm and broad emission from Mn^{2+} centered at around 595 nm (Figure 1a), and the bulk PL decay dynamics (Figure S3) of the microplates are consistent with reported ensemble average properties of nanocrystal Mn:$CsPbCl_3$.[3,5−7,9,19]

To acquire TRCL images, CL lifetime acquisition is implemented via electronic beam blanking and collecting emitted light in time bins on a data acquisition card.[41] Because the Mn^{2+} transition is forbidden, the anticipated lifetime is on the order of a millisecond, so data are collected at a single pixel, ranging in length from 85 to 165 nm, by exciting the corresponding region for 3.0 to 3.5 ms before blanking the beam for a 10 ms acquisition time, after which the beam is moved to the next pixel. CL photons are collected for the full duration of an experiment (Figure 1e), binned in 2 μs intervals, and can be interpreted in the following ways. The data acquired when the beam is blanked are normalized, fit to two exponential decays, and deconvolved from the effects of the finite-duration excitation (Figure S1). A CL intensity image can also be generated simultaneously by integrating all photons emitted pixel by pixel.

Even before analyzing TRCL data, the CL intensity images, generated by integrating the photons emitted from the sample irrespective of the time of emission, show intriguing results. First, we observe mostly spatially homogeneous perovskite emission intensity. The small increase of the signal at the edge (Figure 2b,e) mimics the SE signal (Figure 2a,e) and can be attributed to edge effects that are well-known in electron microscopy. In comparison, the intensity of the Mn^{2+} CL image is approximately two to 10 times greater at the edge than the middle region of the perovskite microplates (Figure 2c,e). The increased edge Mn^{2+} CL intensity is reproducible across more than 30 samples. To readily compare the edge and middle region of the microplates, we sequentially threshold, segment, and aggregate the data separately for each of these two regions (Figure 2d, Figure S2). Using STEM-EDS to perform elemental mapping, we find that the concentration of Mn^{2+} is uniform across the microplate to within the spatial resolution and sensitivity of the measurement (Figure S4). This result suggests that the enhanced CL intensity at the edges is not caused by a local increase in the Mn^{2+} concentration.

TRCL imaging provides more insight into the increase in Mn^{2+} emission intensity at the microplate edges. In the Mn^{2+} TRCL, we observe a biexponential decay of the form $I(t) = a_1 \times e^{-t/\tau_1} + a_2 \times e^{-t/\tau_2}$. The biexponential decay is present in both edge and middle regions with the same time constants, τ_1 = 0.2 ms and τ_2 = 1 ms (Figures 2f). The most significant difference between the edge and the middle is that a_2, the contribution of the longer lifetime component, is approximately 3-fold higher at the edge (Figure 2g). In comparison, a_1, the contribution from the short lifetime component, differs very little between the edge and middle. The increase in a_2 manifests as a longer average lifetime and is consistent with a higher total number of emitted photons at the edge (Figure 2c,f). Because the CL experiment probes a finite generation volume (Figure 1c), measurements at each of the middle and edge both contain some combination of near-surface and bulk material contributions. The edge of perovskite microplates has a higher contribution from the near-surface region due to the inclusion of both the top and side faces, so we attribute the larger value of a_2 at the edge to an even larger value of a_2 in the near-surface region.

Explaining this difference in TRCL requires developing a hypothesis for why the TRCL of the microplates exhibits a biexponential decay and why a_2 differs between the edge and middle of the microplate while a_1, τ_1, and τ_2 are the same in both regions. The explanation that is most consistent with a differing a_2 and uniform a_1 is the presence of two different Mn^{2+} populations that each independently contribute to the overall signal, with their own respective lifetimes, τ_1 and τ_2. We associate one population with τ_1 and the other with τ_2. Because both lifetimes of the Mn^{2+} luminescence are several orders of magnitude longer than the time scales associated with perovskite radiative recombination, self-absorption and re-emission, trapping, or energy transfer, each of the two different Mn^{2+} lifetimes is most likely caused by a distinct property that is directly associated with the Mn^{2+} ions and their surroundings. To assign the independent populations, we compare the two lifetimes. The longer lifetime τ_2 is likely due to a less perturbed, intrinsic Mn^{2+} d−d transition, heretofore labeled Mn^{2+}_{Intr}, which is virtually symmetry forbidden. This assignment is consistent with the Mn^{2+} lifetime previously observed in Mn:$CsPbCl_3$ nanocrystals.[3,5−7,9,20] We suggest that τ_1 is shorter because it arises from a distortion to the Mn^{2+} symmetry environment and heretofore call this population Mn^{2+}_{Dist}. Such a distortion to the Mn^{2+} would decrease the intrinsic octahedral symmetry, which would also decrease the "forbidden" nature of the transition. Biexponential decays in Mn:$CsPbCl_3$ have been previously measured in PL and were suggested to be caused by the presence of Mn−Mn coupled pairs,[10] surface-exposed Mn^{2+},[20] or other trap states.[9] Surface-exposed Mn^{2+} is unlikely to contribute greatly to the overall TRCL signal, since the volume probed in the CL experiment would geometrically contain only a small contribution from the atomic layer at the surface, so Mn−Mn coupled pairs or other trap states would be more likely sources of Mn^{2+}_{Dist}. In summary, we propose that a Mn^{2+}_{Dist} population with $a_1 = a_{Dist}$ is responsible for $\tau_1 = \tau_{Dist}$ and that a Mn^{2+}_{Intr} population with $a_2 = a_{Intr}$ is responsible for $\tau_2 = \tau_{Intr}$.

To explain the 3-fold increase in the excited population of Mn^{2+}_{Intr} between the edge and center while the excited state population of Mn^{2+}_{Dist} remains constant, we consider the excitation mechanism of CL. The electrons from the e-beam scatter within the material, generating electrons and holes that diffuse and undergo radiative recombination to emit a photon. Mn^{2+}_{Intr} luminescence necessarily requires the encounter of an electron and a hole at a Mn^{2+}_{Intr} site. While most treatments of this process describe excitonic energy transfer from the perovskite to the Mn^{2+}, this has been demonstrated in the more commonly studied nanoparticle form factor, where charge carrier confinement is possible. We speculate that, due to the low exciton binding energy in bulk microplates, the charge carriers can instead arrive independently on the Mn^{2+} center. This encounter could be made more probable if charge carriers could be preferentially localized near Mn^{2+} ions. One possible way that this could occur is for a charge carrier to spend more time near a Mn^{2+} site, for instance due to a proximal trap site, such as a halide vacancy. If the concentration of such traps were to increase with proximity to the plate surface then the probability of recombination at

https://dx.doi.org/10.1021/acs.jpclett.0c00574
J. Phys. Chem. Lett. 2020, 11, 2624−2629

Mn^{2+} dopants could also increase, in turn increasing the excited state population, a_2, near the plate surface (Figure 3).

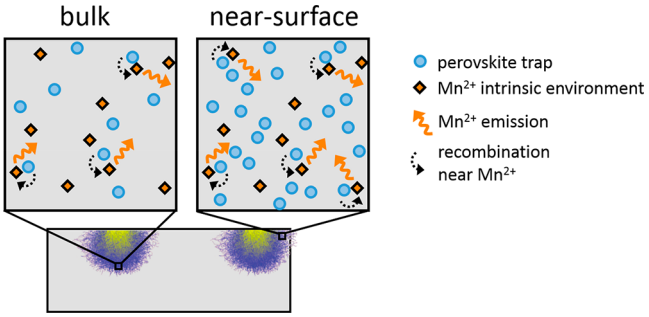

Figure 3. Proposed model for the observed differences between bulk and near-surface. Mn^{2+} dopants (orange diamonds) are present at a constant concentration, while perovskite traps (light blue circles), which are present at varying concentrations, control the relative proportion of Mn^{2+} emission.

In the bulk, a lower trap density would determine a lower baseline probability that a trap and a Mn^{2+} were within a distance small enough to enhance recombination on Mn^{2+} (Figure 3). This reasoning is supported by bulk PL measurements on nano- and microcrystals of Mn^{2+} doped $CsPbCl_3$ that identify a trap-assisted mechanism for energy transfer from the perovskite to the Mn^{2+}.[28,29,42,43] Importantly, the region near perovskite surfaces can be complex, with different properties than for the bulk material. Thus, other near-surface associated behaviors of the perovskite could also plausibly lead to more efficient electron−hole recombination on the Mn^{2+}. Consistent with the assignment of a_1 to the Mn^{2+}_{Dist} population, the unchanging value for a_1 at the edge and middle could be explained in the case that the number of available Mn−Mn pairs or of other features that reduce the octahedral symmetry of the Mn^{2+} were much smaller than the number of electrons and holes available to excite them.

There are two key features of the experimental design that enabled the above findings—the combination of TRCL imaging and the microplate sample geometry. TRCL, as compared to CL intensity alone, gives access to a high spatial resolution photophysical map, which here allows us to distinguish the detailed nature of the difference in CL intensity between the edge and center of the Mn-doped perovskite material. The microplate sample geometry, combined with the spatial context that imaging provides, enables us to furthermore distinguish near-surface and bulk contributions to the CL signal, which would not have been possible for much smaller nanocrystals or in ensemble averaged measurements.

Given the hypothesis that defects, which are more prominent near the surface of the microplate, could be implicated in the enhanced luminescence found at the edges of the material, an interesting consequence to note is that defects could play a positive, rather than negative, role in improving luminescence of Mn^{2+} doped perovskites. In particular, this idea suggests that if Mn^{2+} emission is the desired outcome of doping, then nanocrystals would be an optimal functional geometry, given their high surface to volume ratio. In spite of this finding, TRCL imaging on a material form factor different from that of a nanocrystal was required to elucidate this result.

Overall, we have used TRCL imaging as a powerful method for interpreting local variations in dopant decay behavior within the context of the full sample. Specifically, we have shown that TRCL imaging is capable of resolving spatial variations in recombination efficiency, which we suggest are caused by a larger surface trap density in Mn^{2+}-doped metal halide perovskites. There are many parameters that impact the emissive behavior of dopants in perovskites, not all of which are well understood or characterized. To further characterize dopant emission we have shown that lifetime measurements on the nanoscale are an extremely sensitive way to identify changes in luminescence decay caused by variations in the dopant's local environment and facilitate a more incisive interpretation than changes in emission intensity alone. TRCL imaging has the advantage of superior spatial resolution as compared to time-resolved PL imaging (FLIM) and the ability to simultaneously acquire correlated topographical information via secondary electron scattering. In the future, TRCL imaging could be useful more generally to explain the underlying source of nonspatially uniform behavior in other exciting materials, such as diamond and silicon carbide that contain defect centers used as single photon quantum emitters.

■ ASSOCIATED CONTENT

Supporting Information

The Supporting Information is available free of charge at https://pubs.acs.org/doi/10.1021/acs.jpclett.0c00574.

Detailed methods for synthesis and image acquisition, TRCL decay analysis and segmentation method, bulk PL data, EDS spectra and elemental maps, TRCL lifetimes (PDF)

■ AUTHOR INFORMATION

Corresponding Author

Naomi S. Ginsberg − *Department of Chemistry and Department of Physics, University of California, Berkeley, California 94720, United States; Materials Sciences Division and Molecular Biophysics and Integrated Bioimaging Division, Lawrence Berkeley National Laboratory, Berkeley, California 94720, United States; Kavli Energy NanoScience Institute, Berkeley, California 94720, United States; STROBE, NSF Science & Technology Center, Berkeley, California 94720, United States;* orcid.org/0000-0002-5660-3586; Email: nsginsberg@berkeley.edu

Authors

Rebecca B. Wai − *Department of Chemistry, University of California, Berkeley, California 94720, United States; STROBE, NSF Science & Technology Center, Berkeley, California 94720, United States*

Namrata Ramesh − *Department of Physics, University of California, Berkeley, California 94720, United States; STROBE, NSF Science & Technology Center, Berkeley, California 94720, United States*

Clarice D. Aiello − *Department of Chemistry, University of California, Berkeley, California 94720, United States*

Jonathan G. Raybin − *Department of Chemistry, University of California, Berkeley, California 94720, United States; STROBE, NSF Science & Technology Center, Berkeley, California 94720, United States*

Steven E. Zeltmann − *Department of Materials Science and Engineering, University of California, Berkeley, California 94720, United States; STROBE, NSF Science & Technology Center, Berkeley, California 94720, United States*

https://dx.doi.org/10.1021/acs.jpclett.0c00574
J. Phys. Chem. Lett. 2020, 11, 2624−2629

Connor G. Bischak − *Department of Chemistry, University of California, Berkeley, California 94720, United States;* orcid.org/0000-0002-3071-4069
Edward Barnard − *Molecular Foundry, Lawrence Berkeley National Laboratory, Berkeley, California 94720, United States*
Shaul Aloni − *Molecular Foundry, Lawrence Berkeley National Laboratory, Berkeley, California 94720, United States*
D. Frank Ogletree − *Molecular Foundry, Lawrence Berkeley National Laboratory, Berkeley, California 94720, United States*
Andrew M. Minor − *Department of Materials Science and Engineering, University of California, Berkeley, California 94720, United States; Molecular Foundry and National Center for Electron Microscopy, Molecular Foundry, Lawrence Berkeley National Laboratory, Berkeley, California 94720, United States; STROBE, NSF Science & Technology Center, Berkeley, California 94720, United States*

Complete contact information is available at: https://pubs.acs.org/10.1021/acs.jpclett.0c00574

Notes

The authors declare no competing financial interest.

■ ACKNOWLEDGMENTS

We thank M. Delor and J. Utterback for helpful discussions regarding the interpretation of Mn^{2+} lifetimes and mechanisms. CL, STEM-EDS, all additional characterization and primary analysis have been supported by STROBE, A National Science Foundation Science & Technology Center under Grant No. DMR 1548924. Latter analysis and manuscript preparation were supported by the 'Photonics at Thermodynamic Limits' Energy Frontier Research Center funded by the U.S. Department of Energy (DOE), Office of Science, Office of Basic Energy Sciences, under award DE-SC0019140. The CL imaging at the Lawrence Berkeley Lab Molecular Foundry and the TEM imaging at the National Center for Electron Microscopy were performed as part of the Molecular Foundry user program, supported by the Office of Science, Office of Basic Energy Sciences, of the U.S. Department of Energy under Contract No. DE-AC02-05CH11231. R.B.W and C.G.B. acknowledge NSF Graduate Research Fellowships (No. DGE1106400), and N.S.G. acknowledges an Alfred P. Sloan Research Fellowship, a David and Lucile Packard Foundation Fellowship for Science and Engineering, and a Camille and Henry Dreyfus Teacher-Scholar Award.

■ REFERENCES

(1) Guria, A. K.; Dutta, S. K.; Adhikari, S. D.; Pradhan, N. Doping Mn2+ in Lead Halide Perovskite Nanocrystals: Successes and Challenges. *ACS Energy Lett.* **2017**, *2*, 1014−1021.
(2) Das Adhikari, S.; Guria, A. K.; Pradhan, N. Insights of Doping and the Photoluminescence Properties of Mn-Doped Perovskite Nanocrystals. *J. Phys. Chem. Lett.* **2019**, *10*, 2250−2257.
(3) Parobek, D.; Roman, B. J.; Dong, Y.; Jin, H.; Lee, E.; Sheldon, M.; Son, D. H. Exciton-to-Dopant Energy Transfer in Mn-Doped Cesium Lead Halide Perovskite Nanocrystals. *Nano Lett.* **2016**, *16*, 7376−7380.
(4) Liu, W.; Lin, Q.; Li, H.; Wu, K.; Robel, I.; Pietryga, J. M.; Klimov, V. I. Mn2+-Doped Lead Halide Perovskite Nanocrystals with Dual-Color Emission Controlled by Halide Content. *J. Am. Chem. Soc.* **2016**, *138*, 14954−14961.
(5) Mir, W. J.; Jagadeeswararao, M.; Das, S.; Nag, A. Colloidal Mn-Doped Cesium Lead Halide Perovskite Nanoplatelets. *ACS Energy Lett.* **2017**, *2*, 537−543.
(6) Lin, C. C.; Xu, K. Y.; Wang, D.; Meijerink, A. Luminescent Manganese-Doped CsPbCl 3 Perovskite Quantum Dots. *Sci. Rep.* **2017**, *7*, 45906.
(7) Liu, H.; Wu, Z.; Shao, J.; Yao, D.; Gao, H.; Liu, Y.; Yu, W.; Zhang, H.; Yang, B. CsPbxMn1−XCl3 Perovskite Quantum Dots with High Mn Substitution Ratio. *ACS Nano* **2017**, *11*, 2239−2247.
(8) Zou, S.; Liu, Y.; Li, J.; Liu, C.; Feng, R.; Jiang, F.; Li, Y.; Song, J.; Zeng, H.; Hong, M.; et al. Stabilizing Cesium Lead Halide Perovskite Lattice through Mn(II) Substitution for Air-Stable Light-Emitting Diodes. *J. Am. Chem. Soc.* **2017**, *139*, 11443−11450.
(9) Yuan, X.; Ji, S.; De Siena, M. C.; Fei, L.; Zhao, Z.; Wang, Y.; Li, H.; Zhao, J.; Gamelin, D. R. Photoluminescence Temperature Dependence, Dynamics, and Quantum Efficiencies in Mn2+-Doped CsPbCl3 Perovskite Nanocrystals with Varied Dopant Concentration. *Chem. Mater.* **2017**, *29*, 8003−8011.
(10) De, A.; Mondal, N.; Samanta, A. Luminescence Tuning and Exciton Dynamics of Mn-Doped CsPbCl3 Nanocrystals. *Nanoscale* **2017**, *9*, 16722−16727.
(11) Mir, W. J.; Swarnkar, A.; Nag, A. Postsynthesis Mn-Doping in CsPbI3 Nanocrystals to Stabilize the Black Perovskite Phase. *Nanoscale* **2019**, *11*, 4278−4286.
(12) Dastidar, S.; Egger, D. A.; Tan, L. Z.; Cromer, S. B.; Dillon, A. D.; Liu, S.; Kronik, L.; Rappe, A. M.; Fafarman, A. T. High Chloride Doping Levels Stabilize the Perovskite Phase of Cesium Lead Iodide. *Nano Lett.* **2016**, *16*, 3563−3570.
(13) Zhu, J.; Yang, X.; Zhu, Y.; Wang, Y.; Cai, J.; Shen, J.; Sun, L.; Li, C. Room-Temperature Synthesis of Mn-Doped Cesium Lead Halide Quantum Dots with High Mn Substitution Ratio. *J. Phys. Chem. Lett.* **2017**, *8*, 4167−4171.
(14) Biswas, A.; Bakthavatsalam, R.; Kundu, J. Efficient Exciton to Dopant Energy Transfer in Mn2+-Doped (C4H9NH3)2PbBr4 Two-Dimensional (2D) Layered Perovskites. *Chem. Mater.* **2017**, *29*, 7816−7825.
(15) Chen, D.; Fang, G.; Chen, X.; Lei, L.; Zhong, J.; Mao, Q.; Zhou, S.; Li, J. Mn-Doped CsPbCl3 Perovskite Nanocrystals: Solvothermal Synthesis, Dual-Color Luminescence and Improved Stability. *J. Mater. Chem. C* **2018**, *6*, 8990−8998.
(16) Xu, K.; Vliem, J. F.; Meijerink, A. Long-Lived Dark Exciton Emission in Mn-Doped CsPbCl3 Perovskite Nanocrystals. *J. Phys. Chem. C* **2019**, *123*, 979−984.
(17) Rossi, D.; Parobek, D.; Dong, Y.; Son, D. H. Dynamics of Exciton−Mn Energy Transfer in Mn-Doped CsPbCl3 Perovskite Nanocrystals. *J. Phys. Chem. C* **2017**, *121*, 17143−17149.
(18) Huang, G.; Wang, C.; Xu, S.; Zong, S.; Lu, J.; Wang, Z.; Lu, C.; Cui, Y. Postsynthetic Doping of MnCl2Molecules into Preformed CsPbBr3 Perovskite Nanocrystals via a Halide Exchange-Driven Cation Exchange. *Adv. Mater.* **2017**, *29*, 1700095.
(19) Das Adhikari, S.; Dutta, S. K.; Dutta, A.; Guria, A. K.; Pradhan, N. Chemically Tailoring the Dopant Emission in Manganese-Doped CsPbCl3 Perovskite Nanocrystals. *Angew. Chem., Int. Ed.* **2017**, *56*, 8746−8750.
(20) Xu, K.; Lin, C. C.; Xie, X.; Meijerink, A. Efficient and Stable Luminescence from Mn2+ in Core and Core−Isocrystalline Shell CsPbCl3 Perovskite Nanocrystals. *Chem. Mater.* **2017**, *29*, 4265−4272.
(21) Chen, D.; Fang, G.; Chen, X. Silica-Coated Mn-Doped CsPb(Cl/Br)3 Inorganic Perovskite Quantum Dots: Exciton-to-Mn Energy Transfer and Blue-Excitable Solid-State Lighting. *ACS Appl. Mater. Interfaces* **2017**, *9*, 40477−40487.
(22) He, T.; Li, J.; Ren, C.; Xiao, S.; Li, Y.; Chen, R.; Lin, X. Strong Two-Photon Absorption of Mn-Doped $CsPbCl_3$ Perovskite Nanocrystals. *Appl. Phys. Lett.* **2017**, *111*, 211105.
(23) Fei, L.; Yuan, X.; Hua, J.; Ikezawa, M.; Zeng, R.; Li, H.; Masumoto, Y.; Zhao, J. Enhanced Luminescence and Energy Transfer in Mn2+ Doped CsPbCl3−xBrx Perovskite Nanocrystals. *Nanoscale* **2018**, *10*, 19435−19442.
(24) Li, Z.-J.; Hofman, E.; Davis, A. H.; Khammang, A.; Wright, J. T.; Dzikovski, B.; Meulenberg, R. W.; Zheng, W. Complete Dopant

Substitution by Spinodal Decomposition in Mn-Doped Two-Dimensional CsPbCl3 Nanoplatelets. *Chem. Mater.* **2018**, *30*, 6400−6409.
(25) Ji, S.; Yuan, X.; Li, J.; Hua, J.; Wang, Y.; Zeng, R.; Li, H.; Zhao, J. Photoluminescence Lifetimes and Thermal Degradation of Mn2+-Doped CsPbCl3 Perovskite Nanocrystals. *J. Phys. Chem. C* **2018**, *122*, 23217−23223.
(26) Das Adhikari, S.; Behera, R. K.; Bera, S.; Pradhan, N. Presence of Metal Chloride for Minimizing the Halide Deficiency and Maximizing the Doping Efficiency in Mn(II)-Doped CsPbCl3 Nanocrystals. *J. Phys. Chem. Lett.* **2019**, *10*, 1530−1536.
(27) Dutta, S. K.; Pradhan, N. Coupled Halide-Deficient and Halide-Rich Reaction System for Doping in Perovskite Armed Nanostructures. *J. Phys. Chem. Lett.* **2019**, *10*, 6788−6793.
(28) Pinchetti, V.; Anand, A.; Akkerman, Q. A.; Sciacca, D.; Lorenzon, M.; Meinardi, F.; Fanciulli, M.; Manna, L.; Brovelli, S. Trap-Mediated Two-Step Sensitization of Manganese Dopants in Perovskite Nanocrystals. *ACS Energy Lett.* **2019**, *4*, 85−93.
(29) Wei, Q.; Li, M.; Zhang, Z.; Guo, J.; Xing, G.; Sum, T. C.; Huang, W. Efficient Recycling of Trapped Energies for Dual-Emission in Mn-Doped Perovskite Nanocrystals. *Nano Energy* **2018**, *51*, 704−710.
(30) Berezin, M. Y.; Achilefu, S. Fluorescence Lifetime Measurements and Biological Imaging. *Chem. Rev.* **2010**, *110*, 2641−2684.
(31) Cole, M. J.; Siegel, J.; Webb, S. E. D.; Jones, R.; Dowling, K.; Dayel, M. J.; Parsons-Karavassilis, D.; French, P. M. W.; Lever, M. J.; Sucharov, L. O. D.; et al. Time-Domain Whole-Field Fluorescence Lifetime Imaging with Optical Sectioning. *J. Microsc.* **2001**, *203*, 246−257.
(32) Bastiaens, P. I. H.; Squire, A. Fluorescence Lifetime Imaging Microscopy: Spatial Resolution of Biochemical Processes in the Cell. *Trends Cell Biol.* **1999**, *9*, 48−52.
(33) Bischak, C. G.; Hetherington, C. L.; Wu, H.; Aloni, S.; Ogletree, D. F.; Limmer, D. T.; Ginsberg, N. S. Origin of Reversible Photoinduced Phase Separation in Hybrid Perovskites. *Nano Lett.* **2017**, *17*, 1028−1033.
(34) Bischak, C. G.; Wong, A. B.; Lin, E.; Limmer, D. T.; Yang, P.; Ginsberg, N. S. Tunable Polaron Distortions Control the Extent of Halide Demixing in Lead Halide Perovskites. *J. Phys. Chem. Lett.* **2018**, *9*, 3998−4005.
(35) Duong, T.; Mulmudi, H. K.; Shen, H.; Wu, Y.; Barugkin, C.; Mayon, Y. O.; Nguyen, H. T.; Macdonald, D.; Peng, J.; Lockrey, M.; et al. Structural Engineering Using Rubidium Iodide as a Dopant under Excess Lead Iodide Conditions for High Efficiency and Stable Perovskites. *Nano Energy* **2016**, *30*, 330−340.
(36) Dar, M. I.; Jacopin, G.; Hezam, M.; Arora, N.; Zakeeruddin, S. M.; Deveaud, B.; Nazeeruddin, M. K.; Grätzel, M. Asymmetric Cathodoluminescence Emission in CH3NH3PbI3−XBrx Perovskite Single Crystals. *ACS Photonics* **2016**, *3*, 947−952.
(37) Atre, A. C.; Brenny, B. J. M.; Coenen, T.; García-Etxarri, A.; Polman, A.; Dionne, J. A. Nanoscale Optical Tomography with Cathodoluminescence Spectroscopy. *Nat. Nanotechnol.* **2015**, *10*, 429−436.
(38) Cortecchia, D.; Lew, K. C.; So, J.-K.; Bruno, A.; Soci, C. Cathodoluminescence of Self-Organized Heterogeneous Phases in Multidimensional Perovskite Thin Films. *Chem. Mater.* **2017**, *29*, 10088−10094.
(39) Ponce, F. A.; Srinivasan, S.; Bell, A.; Geng, L.; Liu, R.; Stevens, M.; Cai, J.; Omiya, H.; Marui, H.; Tanaka, S. Microstructure and Electronic Properties of InGaN Alloys. *Phys. Status Solidi B* **2003**, *240*, 273−284.
(40) Moerland, R. J.; Weppelman, I. G. C.; Garming, M. W. H.; Kruit, P.; Hoogenboom, J. P. Time-Resolved Cathodoluminescence Microscopy with Sub-Nanosecond Beam Blanking for Direct Evaluation of the Local Density of States. *Opt. Express* **2016**, *24*, 24760−24772.
(41) Aiello, C. D.; Pickel, A. D.; Barnard, E.; Wai, R. B.; Monachon, C.; Wong, E.; Aloni, S.; Ogletree, D. F.; Dames, C.; Ginsberg, N. Cathodoluminescence-Based Nanoscopic Thermometry in a Lanthanide-Doped Phosphor. 2018, arXiv: physics/1810.07581 arXiv.org e-Print archive. https://arxiv.org/abs/1810.07581 (accessed October 23, 2018).
(42) Luo, B.; Guo, Y.; Li, X.; Xiao, Y.; Huang, X.; Zhang, J. Z. Efficient Trap-Mediated Mn2+ Dopant Emission in Two Dimensional Single-Layered Perovskite (CH3CH2NH3)2PbBr4. *J. Phys. Chem. C* **2019**, *123*, 14239−14245.
(43) Sun, Q.; Wang, S.; Zhao, C.; Leng, J.; Tian, W.; Jin, S. Excitation-Dependent Emission Color Tuning from an Individual Mn-Doped Perovskite Microcrystal. *J. Am. Chem. Soc.* **2019**, *141*, 20089.

https://dx.doi.org/10.1021/acs.jpclett.0c00574
J. Phys. Chem. Lett. 2020, 11, 2624−2629